Article:
Mora, Nicolas, Flintoft, Ian David orcid.org/0000-0003-3153-8447, Dawson, Linda et al. (5 more authors) (2016) Experimental characterization of the response of an electrical and communication raceway to IEMI. IEEE Transactions on Electromagnetic Compatibility. pp. 494-505. ISSN 0018-9375

https://doi.org/10.1109/TEMC.2015.2510423

Experimental Characterization of the Response of an Electrical and Communication Raceway to IEMI

Nicolas Mora[1], Ian D. Flintoft[2], Linda Dawson[2], John F. Dawson[2], Farhad Rachidi[1], Marcos Rubinstein[3], Andy C. Marvin[2], Pierre Bertholet[4] and Markus Nyffeler[4]

[1] *EMC Laboratory of the Swiss Federal Institute of Technology (EPFL), EPFL-SCI-STI-FR, Station 11, 1015 Lausanne, Switzerland.*
[2] *Department of Electronics, University of York, Heslington, York YO10 5DD, UK.*
[3] *University of Applied Sciences of Western Switzerland, 1400 Yverdon-les-Bains, Switzerland.*
[4] *HPE Laboratory of the Swiss Federal Office for Defence Procurement (Armasuisse), Feuerwerkerstrasse 39, 3602 Thun, Switzerland.*

Published in IEEE Transaction on Electromagnetic Compatibility, vol. 58, no. 2, pp. 494-505, Apr. 2016.

Accepted for publication 02/12/2015

DOI: 10.1109/TEMC.2015.2510423

URL: http://ieeexplore.ieee.org/xpl/articleDetails.jsp?arnumber=7383289

Experimental Characterization of the Response of an Electrical and Communication Raceway to IEMI

Nicolas Mora, *Member, IEEE*, Ian D. Flintoft, *Senior Member, IEEE*, Linda Dawson, John F. Dawson, *Member, IEEE*, Farhad Rachidi, *Fellow, IEEE*, Marcos Rubinstein, *Fellow, IEEE*, Andy C. Marvin, *Fellow, IEEE*, Pierre Bertholet, Markus Nyffeler

***Abstract*—This paper reports the results of two experimental campaigns aimed at studying the high-frequency response of a raceway containing low voltage power, telephone, and Ethernet cables, to external electromagnetic field illumination. The raceway was tested against HPEM transients inside a GTEM cell and low power fields inside a reverberation chamber (RC). The HPEM tests revealed that the low voltage power cables have the greatest coupling under a hyperband illumination, compared to telephone and Ethernet cables. The RC tests allowed the determination of statistical transfer functions from random incident field configurations into DM voltage in cable loads. The responses were found to be governed by the raceway under test at the lower frequencies (below 1 GHz). Between 0.2-1 GHz, the raceway gives about 10 dB higher coupling than a short patch cable. The difference is even greater at lower frequencies and for shielded cables. In the frequency band 1-3 GHz, little difference was observed between short patch cables and the full raceway, but both were still significantly higher than direct coupling to the measurement card. Beyond 3 GHz, the coupling is clearly dominated by the terminal equipment. The experiments performed in this work provide a better understanding of the expected induced voltages and currents in commercial cable systems when exposed to IEMI-like signals.**

***Index Terms*—Intentional electromagnetic interference, immunity testing, EMP radiation effects, reverberation chambers, electromagnetic Coupling, cable shielding**

Manuscript received June 1, 2015. This study was financially supported by the European Community's 7th Framework Programme under the grant agreement 285257, STRUCTURES (Strategies for the improvement of critical infrastructure resilience to electromagnetic Attacks), Swisselectric Research and Armasuisse.

N. Mora, and F. Rachidi are with the EMC Laboratory of the Swiss Federal Institute of Technology (EPFL), EPFL-SCI-STI-FR, Station 11, 1015 Lausanne, Switzerland (e-mail: nicolas.mora@epfl.ch; farhad.rachidi@epfl.ch).

I. D. Flintoft, L. Dawson, J. F. Dawson, and A. C. Marvin are with the Department of Electronics, University of York, York YO10 5DD, U.K. (e-mail: ian.flintoft@york.ac.uk; l.dawson@york.ac.uk; john.dawson@york.ac.uk; andy.marvin@york.ac.uk).

M. Rubinstein is with the University of Applied Sciences of Western Switzerland, 1400 Yverdon-les-Bains, Switzerland (e-mail: marcos.rubinstein@heig-vd.ch).

P. Bertholet, and M. Nyffeler are with the HPE Laboratory of the Swiss Federal Office for Defence Procurement (Armasuisse), Feuerwerkerstrasse 39, 3602 Thun, Switzerland (e-mail:pierre.bertholet@armasuisse.ch; markus.nyffeler@armasuisse.ch).

I. Introduction

Hardening of infrastructures against intentional electromagnetic interference (IEMI) requires a prior knowledge of the nature of the expected perturbations arriving to the protected equipment. Among the typical parameters of interest are the amplitude and frequency content of the induced current or voltage at the equipment inputs.

Recent studies have shown the possibility of interrupting the normal functioning of IT networks using High Power Electromagnetic (HPEM) interferences through the low voltage power (LVP) network [1, 2] and the local area network (LAN) cables [1-3]. In [1, 2], mesoband sources [4] of about 60 kV/m were used to temporarily interrupt an Ethernet switch after illuminating its LVP cable in an anechoic chamber (AC). Similar tests with hyperband fields of 44 kV/m inside a Gigahertz Transverse Electromagnetic (GTEM) Cell [1, 2], and 6.6 kV/m in a TEM Cell [3] have shown to slow down or permanently break the data transfer of the switch, depending on the pulse repetition frequency of the source.

Predictions of the coupled voltage and current levels at the cable terminals (input of the equipment) can be obtained with the use of the transmission line (TL) theory (e.g., [5] [6-8]), assuming that the cable parameters are known. The use of TL-based approximation techniques for modeling the propagation of IEMI transients in LVP networks has been studied in [9, 10] where it was shown that uncertainties in the input geometrical and electrical parameters of the exposed line may significantly impact the accuracy of simulated results. The stochastic nature of the impinging field and the wire positions can be included in the predictions (e.g., [11-15]). In particular, TL models of straight wire lines excited by a superposition of random plane waves have been shown to provide results which are in good agreement with experimental data obtained using reverberation chambers (RC) in [11, 12]. The relation between field-to-wire coupling test results obtained in a RC and AC is discussed in [16].

Electromagnetic field coupling to unshielded twisted pairs (TWP) has also been a subject of recent studies (e.g., [7, 17-21]]. It has been shown that accurate predictions for the induced common mode (CM) and differential mode (DM) voltages can be achieved as long as the considered

configurations are relatively simple. On the other hand, DM voltage estimation is very sensitive to less controlled parameters like the twist pitch or a non-integer number of twists, which might lead to inaccurate predictions in realistic scenarios [1, 22]. Other factors including the presence of non-ideal connectors, load imbalance [7, 23], line non-uniformity [24], and improper line terminations [25, 26] substantially contribute to inaccuracies in numerical/analytical predictions. Therefore, experimental results are needed to obtain correct estimates of induced DM signals in TWP cables.

Similar issues occur in the prediction of field coupling to shielded cables where the overall response can be significantly affected by the presence of pigtails, or bad contact resistances between the shields and connectors (see e.g. [27]). Experimental results for shielded cables illuminated inside a RC in [28] have shown that modifications in the range of tens of dBs are obtained in the voltage response of a shielded cable due to a change of the connector type.

This paper presents the results of two experimental campaigns carried out to study the levels of induced DM voltage and CM current in typical configurations of LVP, telephone (TEL) and LAN installations inside an office, due to an external electromagnetic field illumination representative of IEMI. The first test consists of the illumination of a commercial raceway with a HPEM field inside a GTEM cell. In the second test, the same raceway was illuminated with a CW signal in a RC.

The idea of testing with these two separate methods was two-fold: (i) We wish to estimate the expected conducted disturbances at the input of equipment connected to the cables due to a HPEM illumination, without having to model the complete setup in a full wave or transmission line environment; (ii) To be able to generalize the obtained results for the case of multiple angles of incidence and non-uniform illumination, with statistically plausible data. The first method is useful for understanding the induced levels in the time domain, whereas the second is useful to assess the general behavior of the assemblies in the frequency domain. The experiments have been performed with the intention of providing a general idea of the coupling levels and this is why we have used representative cables and structures as in realistic scenarios.

The paper is organized as follows. Section II presents the device under test, namely a typical electrical and communications raceway including several types of cables that are found in commercial buildings. Section III presents the transient HPEM illumination setup inside a GTEM cell while Section IV presents the low power test setup inside a RC. The obtained results with relevant discussion are presented in Sections V and VI. Finally, summary and conclusions are presented in Section VII.

II. Device Under Test

This section describes the electrical and communication raceway under test and the measurement interface cards that were specifically designed to access the induced signals in individual conductors.

A. Raceway description

The device under test is a 200-cm long raceway containing several LVP, LAN, and TEL cables, typical of a civilian office environment. A schematic diagram representing the cablings inside the raceway is shown in Fig. 1.

1) Low voltage power cabling

The LVP cabling is composed of 4 TT 3 x 1.5 mm^2 cables terminated with triple-power sockets of SEV 1011 type. The LVP cables contain three coated wires corresponding to the phase, neutral, and ground conductors of the distribution network and are supposed to withstand a DM peak voltage of 1 kV before dielectric breakdown. The four power sockets were labeled from left to right as AC1, AC2, AC3, and AC4, respectively.

The power cables were connected in a star configuration with one end connected to the sockets and the other end to a junction box represented by a green square in Fig. 1. The junction box can be also used to connect the test raceway to external 220V/ 50Hz power lines. Since the study does not require the test of the equipment in a powered state, the power cables were left isolated from the external power network.

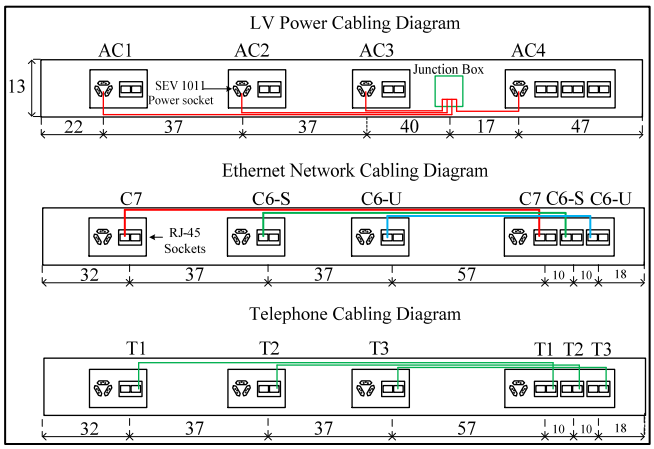

Fig. 1 Schematic diagram of the cablings inside the test raceway. Distances are in cm and not to scale.

2) Ethernet network cabling

The Ethernet network cabling is composed of 3 LAN cables terminated at both ends with RJ-45 sockets. Each LAN cable contains 4 TWPs. Each TWP is made of 2 coated copper wires that may contain a shielding screen to avoid interference with the other pairs of the bundle. The 4 TWPs are grouped into a single bundle that may be also shielded to avoid interference with the environment.

Three different LAN cable categories were used (shown as red, green and blue lines in the schematic of Fig. 1) as follows:

- C7: Category 7 S/FTP cable
- C6-S: Category 6 SF/UTP cable
- C6-U: Category 6 U/UTP cable

A summary of the properties of the used LAN cables, according the manufacturer datasheets, is shown in Table I. The RJ-45 connectors were labeled according to the LAN cable category.

TABLE I
LAN CABLE SPECIFICATION

Label	Cat.	Class	Bundle shield	TWP shield	Max. Freq. (MHz)
C7	7	F	Braid	Foil	600
C6-S	6	E	Braid-foil	None	450
C6-U	6	E	None	None	300

3) Telephone cabling

The TEL cables were three U72 cables terminated at both ends with RJ-45 sockets. U72 are unshielded cables containing 4 twisted coated wires. According to the manufacturer's datasheet, the maximum usable frequency for this kind of cables is 5 MHz. Notice that in practice, only 2 wires of the U72 cable are required for the telephone connections. The termination sockets of the TEL cable were labeled as T1, T2, and T3, respectively.

B. Measurement interface cards description

The current and voltage measurements performed in this work used two measurement interface cards that were specifically designed to make a transition between the different cable outputs and the 50 Ω input of a measuring oscilloscope or vector network analyzer (VNA). Additionally, the interface cards could also be used as 50 Ω or 100 Ω terminations for unused or floating wires in the cables under test.

A schematic diagram describing the measurement interface cards is shown in Fig. 2.

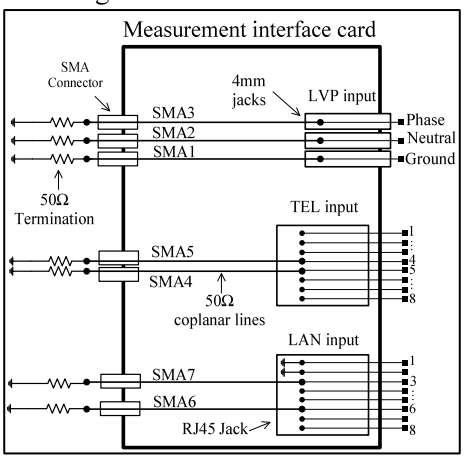

Fig. 2 Schematic diagram of the measurement interface cards.

The measurement card has 3 inputs, namely, the LVP input (phase, neutral, and ground wires), the TEL input (2 wires of the TEL cable connected to pins 4 and 5 of the TEL RJ 45 jack), and the LAN input (8 wires of the LAN cable connected to the LAN RJ-45 jack). The measured signals are transmitted through 50Ω coplanar lines of identical electrical length to seven SMA connectors located at the other end of the card. These connectors serve to connect the measurement channel or to terminate the lines with a 50 Ω load. The DM termination impedance between any pair of SMA connectors is 100 Ω.

Out of the 8 available wires from the LAN cable, only two (pins 3 and 6) were used for measurement. These correspond to the Rx+ and Rx- wires in classical Ethernet networks. Also pins 1 and 2 are connected to the card reference plane. These correspond to the Tx+ and Tx- wires in classical Ethernet networks.

The measurement cards were installed inside a metallic enclosure that provides better shielding than a typical commercial off-the shelf (COTS) product. Representative RJ 45 connectors were used for the TEL and LAN inputs with additional shielding provided by a seal made up with copper tape. The effect of the additional shielding on the RJ-45s will be shown later in Fig. 20. A picture of one of the measurement cards (without the copper tape seal over the RJ 45s) is shown in Fig. 3. There are two additional SMA connectors on the top part of the picture that are connected to a through PCB line that was made for calibrating the delay between the lines due to the FR4 effective permittivity.

III. TRANSIENT HPEM ILLUMINATION SETUP

In this section, the experimental setups for the high power illumination tests inside the GTEM cell are presented.

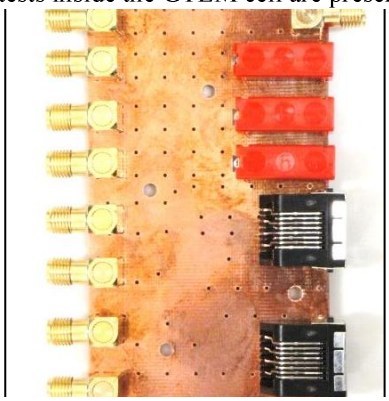

Fig. 3 Top view of the measurement cards without the shielding enclosure. Notice that the shield of the RJ-45 jacks is not continuous.

A. GTEM cell description

The illumination tests were performed in the GTEM cell of Armasuisse (Swiss Defence Procurement Agency) located in the RUAG Defense Labs in Bern. The cell reference is GTEM 3750 fabricated by EMC Baden. A schematic diagram illustrating the dimensions of the cell is presented in Fig. 4. The working volume was 2.5m x 2.5m x 2m.

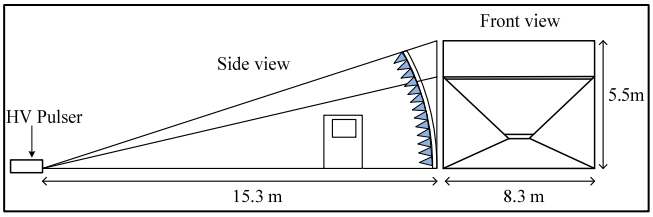

Fig. 4 Front and side view of the GTEM 3750 Cell of Armasuisse.

The input of the GTEM cell was connected to a bipolar 200ps/50kV peak-to-peak amplitude pulser provided by ISL [29]. The pulser was remotely operated using a computer and a fiber optic (FO) communication link. The output of the pulser was connected to the GTEM cell input through an impedance adapter [30].

The electromagnetic field generated in the working volume was characterized using B-dot and D-dot sensors. The voltage

output of the sensors was transmitted through a Fiber optic (FO) Link to a digital oscilloscope. The FO transmitter was located inside the cell, and the FO receiver was installed in a shielded cabin outside the cell.

A summary of the specifications of the used equipment is given in Table II.

TABLE II
GTEM CELL EXPERIMENTAL SETUP CONFIGURATION FOR FIELD MAPPING

Parameter	Description
D-dot max. frequency	1.2 GHz
D-dot max. field	1MV/m
B-dot max. frequency	1.3 GHz
B-dot max. field	2.65kA/m
FO link max. frequency	3.2GHz
Oscilloscope sampling rate	20Gs/s
Oscilloscope max. frequency	6GHz

Several field samples were taken at different positions inside the working volume. The measurements correspond to the average of 6 subsequent shots of the pulser. The generated field was found to be a uniform TEM wave. A plot of a typical measured vertical E-field and horizontal H-field, and their frequency spectra is presented in Fig. 5. In order to check the TEM validity, we have multiplied the magnetic field curve by the free space impedance $\eta = 120\pi$. We have also checked that the field components in the other directions were significantly lower.

The generated E-field is a bipolar hyperband pulse of about 40kV/m peak-to-peak amplitude. Given that the risetime of the D-dot sensor is slower than the driving source risetime (about 230ps), the risetime of the generated field is approximated to the risetime of the pulser, namely 200ps.

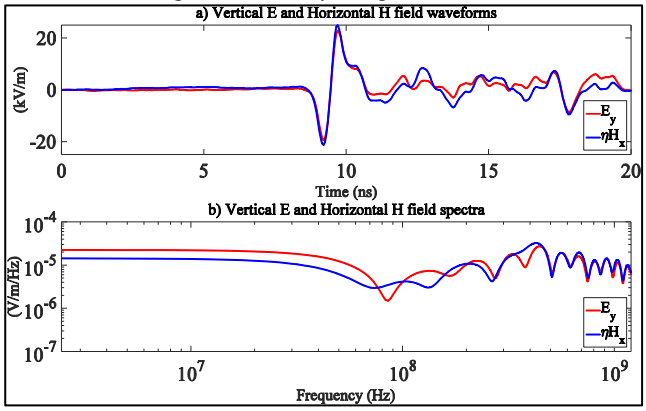

Fig. 5 Waveform and spectrum of the generated vertical E-field and horizontal H-field in the working volume of the GTEM cell. The DC component of the derivative sensors was removed before integration to avoid the offset-induced spurious integration ramp.

B. Common mode current test

A schematic diagram of the common mode current measurement setup is presented in Fig. 6. The raceway was either vertically or horizontally positioned inside the working volume of the GTEM cell in order to test the effect of a normal and grazing incidence of the field. The induced common mode current in the cable under test was measured with a current transformer (CT) connected to a digital oscilloscope through a FO transceiver. The output of the CT was attenuated in order to meet the input requirements of the FO transmitter. The oscilloscope was configured to take the average of 6 subsequent triggers.

The LVP, LAN or TEL lines were connected to the interface cards' inputs, and the common mode current flowing from the output socket of the raceway was measured with the CT. All the SMA ports of the cards were terminated with 50Ω loads during this test. The connection between the cards' input and the raceway sockets was made through patch cords of the same type as the cables under test. For example, during the C7 LAN cable test, the RJ-45 jack of the interface card was connected to the raceway by using a patch cord of category 7 S/FTP.

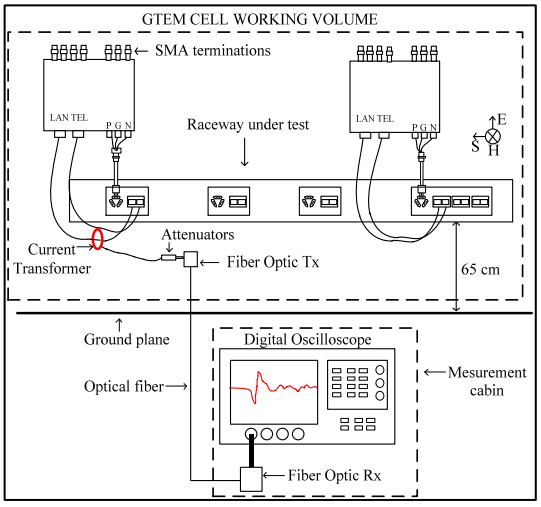

Fig. 6 Schematic diagram of the common mode current test

A picture illustrating the measurement setup with the raceway in the horizontal position is shown in Fig. 7.

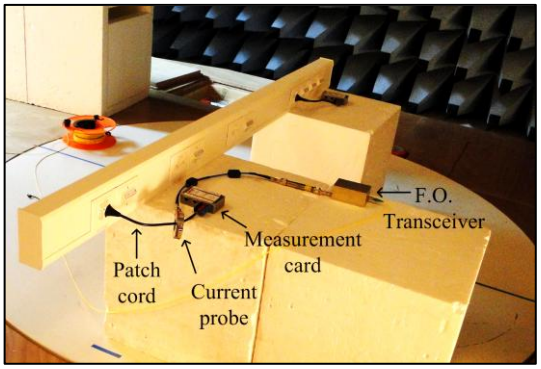

Fig. 7 Picture illustrating the common mode current measurement in the AC1 LVP lines with AC4 loaded by the second interface card; while the raceway was positioned in horizontal position.

C. Differential mode voltage test

A schematic diagram of the DM voltage measurement setup is presented in Fig. 8. The raceway was either vertically or horizontally positioned inside the working volume of the GTEM cell. The induced voltages in two selected wires of the cable under test were measured by connecting the interface cards' outputs to the FO transceiver. The DM voltage between the two wires was determined by calculating the difference between the signals in the two wires. The outputs of the measuring interface card were attenuated in order to meet the input requirements of the FO transmitter. As in the common mode current test, the oscilloscope was configured to take the average of 6 subsequent triggers.

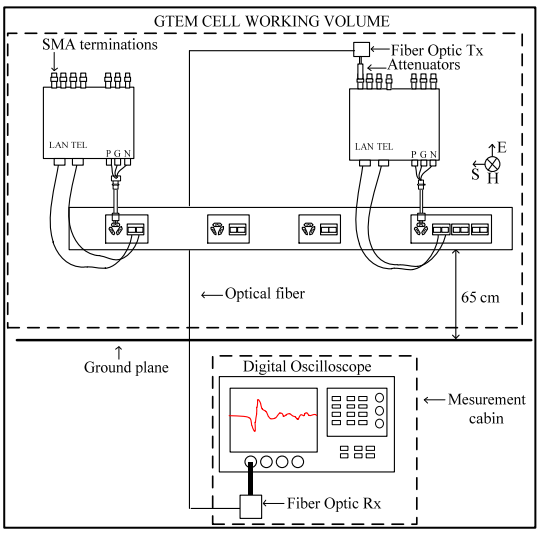

Fig. 8 Schematic diagram of the DM voltage test. The diagram illustrates the measurement of one of the DM lines.

The LVP, LAN or TEL lines were connected to the interface cards' inputs, and the outputs of two SMA ports were connected to the oscilloscope through the FO transceiver. The other SMA ports were terminated with 50Ω loads.

A summary of the equipment configuration for both tests is presented in Table III.

TABLE III
EXPERIMENTAL SETUP CONFIGURATION FOR THE GTEM ILLUMINATION TESTS

Parameter	Description
CT frequency range	1 MHz-1GHz
CT max. pulse current	100A
Fiber optic link max. freq.	3.2GHz
Oscilloscope sampling rate	20Gs/s
Oscilloscope max. freq.	6GHz

IV. REVERBERATION CHAMBER SETUP

A. *Reverberation chamber description*

The RC illumination tests were performed in the chamber located in the Department of Electronics, University of York UK. The 4.70 m x 3.00 m x 2.37 m chamber has a lowest usable frequency (LUF) of about 100 MHz. It is tuned using a mechanical paddle driven by a stepper motor in the chamber roof that is controlled by a PC using a serial interface. The working volume of the chamber at 1 GHz is approximately 2.3 m × 2.7 m × 2.0 m.

The measurements were conducted using a VNA controlled via a GPIB interface from a PC. The setup for the calibration and coupling measurements is shown in Fig. 9. The PC controlled the paddle rotation and an RF switch module located inside the chamber was used to alternate between the two signal wires being measured during each coupling experiment. The switch module has an isolation of more than 70 dB (typically 90 dB) up to 8 GHz.

All the RC measurements reported here were carried out over the frequency band 200 MHz to 6 GHz, collecting 1601 frequency samples at 100 equally spaced positions of the paddle over a full rotation. A full two-port calibration of the VNA, cables and RF switch up to the input ports of the antennas was carried out. The small amplitude and phase imbalance of the two cables from the RF switch unit to the measurement card was calibrated out by de-embedding (in post-processing) an S-parameter error block determined from a separate VNA measurement of the two cables. Hybrid "blade" antennas covering the range 200 MHz to 26 GHz were used to allow the required frequency range to be measured without switching antennas [31].

B. *RC uniformity and calibration*

Where appropriate the test methodology followed the IEC61000-4-21 standard [32]. The electromagnetic field generated inside of the working volume of the chamber was characterized with the raceway and any other equipment in place and the external switch shown in Fig. 9 set to the "power calibration" position. The transmission between the pair of blade antennas was measured and the average power density and hence the mean-square electric field, $\langle |\mathrm{E}^{\mathrm{inc}}|^2 \rangle$, within the working volume determined from

$$\langle S \rangle = \frac{\langle |\mathrm{E}^{\mathrm{inc}}|^2 \rangle}{\eta_0} = \frac{1}{\eta_2^T}\frac{8\pi}{\lambda^2}\langle |\mathrm{S}_{21}|^2 \rangle \frac{|\mathrm{V}_1^+|^2}{Z_0}. \quad (1)$$

Here V_1^+ is the forward voltage of the VNA, η_0 the intrinsic impedance of free-space, Z_0 the VNA port impedance and η_2^T is the total efficiency of the receiving antenna, given by

$$\eta_2^T = \eta_2^{\mathrm{rad}}(1-|\mathrm{S}_{22}^{FS}|^2) \approx (1-|\langle \mathrm{S}_{22} \rangle|^2), \quad (1)$$

where η_2^{rad} is the radiation efficiency of the antenna (due to ohmic and dielectric losses) and S_{22}^{FS} is its free-space reflection coefficient. The statistical error in the fields was about ±0.5 dB [33]. A summary of the required equipment for this test and the specifications are reported in Table IV.

TABLE IV
EQUIPMENT FOR POWER DENSITY CALIBRATION OF RC MEASUREMENTS

Equipment	Description
VNA	Rhode & Schwarz ZVB 20
PC3.5 SOLT cal. kit	Rhode & Schwarz ZV-Z235
Rx/Tx antenna	UoY hybrid "Blade" antenna
RF switch	Mini-circuits MSP2TA-18, DC-18 GHz
Microwave cables	Reynolds Industries 269-0195

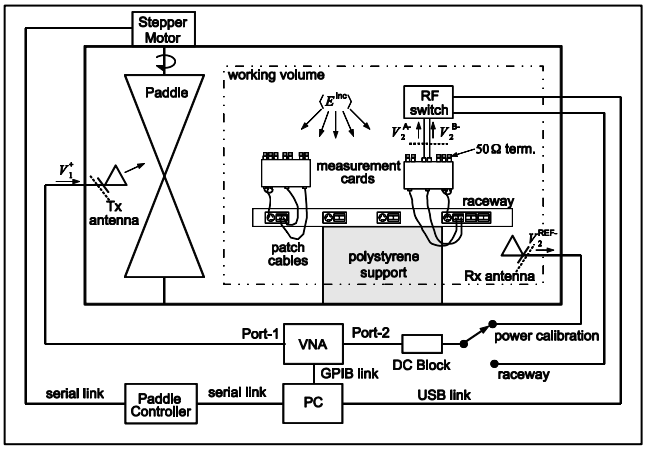

Fig. 9 RC Measurement setup. The dotted lines show the calibration planes of the VNA.

C. *Differential mode coupling tests*

The configuration for coupling measurements was the same

as in Fig. 9, with the external switch (after the DC block) in the "raceway" position. It was essential that the equipment was not disturbed between the power density calibration and raceway measurements in order to obtain accurate results. The RF switch unit was used to allow the measurement of the received voltage into 50 ohms on each wire in a signal pair of a cable, V_1^- and V_2^-, at each paddle angle. The mean-square DM voltage at each paddle position was calculated from

$$\left\langle |\, V_{DM}\,|^2 \right\rangle = \left\langle |\, V_1^- - V_2^-\,|^2 \right\rangle. \qquad (2)$$

Statistical distribution functions for $|\, V_{DM}\,|$ over the different paddle positions can be also obtained. These are expected to have Rayleigh distributions [11, 12, 20, 34].

V. Transient HPEM Illumination Results

A. Common mode current results

CM current measurements were performed in each of the 9 cables (3 LVP, 3 TEL, and 3 LAN) while the raceway was either in the vertical or horizontal position inside the GTEM cell. Notice that in the LVP measurements, the near end measurement card was connected to AC1, AC2, or AC3, while the far end card was always connected to AC4. Depending on the cable under test, different profiles of induced current waveforms were obtained.

1) Typical result

An example of the CM current from a measurement performed in the C7 cable (see Fig. 1) is presented in Fig. 10a. The plot corresponds to a measurement performed while the raceway was in the vertical position. The oscillatory waveform has a peak amplitude of 6 A. The computed frequency spectrum is shown in Fig. 10b. It features several resonant frequencies with a peak at about 50 MHz, an expected behavior for line lengths of the order of meters. Similar curves exhibiting an oscillatory behavior with several resonant frequencies were obtained for the other cables.

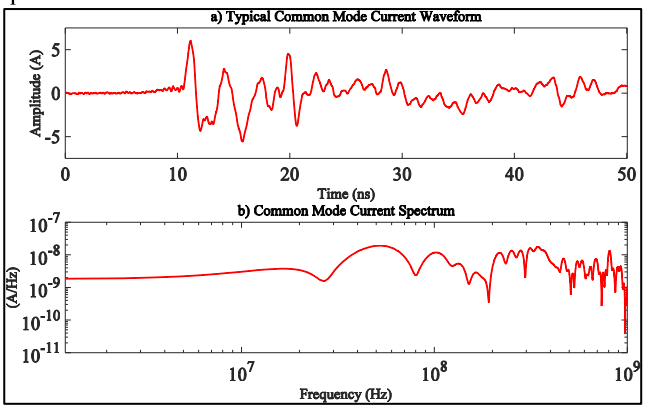

Fig. 10 Example of a current measurement performed in the C7 cable with the raceway in a vertical position. The incident E-field is shown in Fig. 5.

2) Peak amplitudes

A bar plot summarizing the peak amplitudes of the 18 measurements is presented in Fig. 11. The results obtained with the raceway in vertical and horizontal positions are plotted with red and blue bars, respectively. Amplitudes between 1 and 10 A were observed with higher values corresponding to the normal incidence of the field (raceway in the vertical position). Similar current levels and resonant frequencies have been reported for 44kV/m hyperband illuminations [1, 2] and 10-50 kV/m NEMP illuminations [35] of LAN cables.

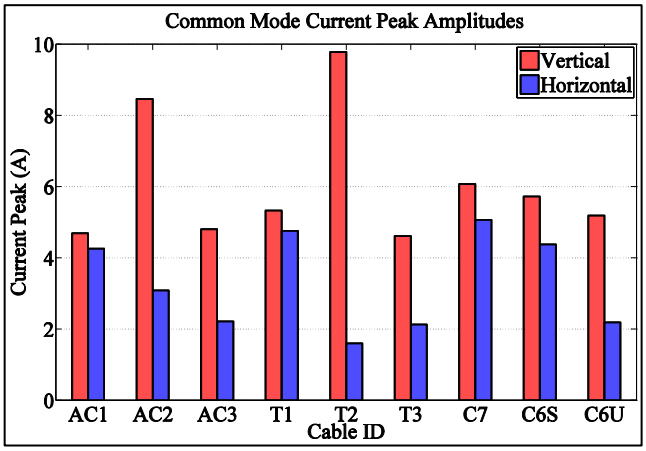

Fig. 11 Bar plot of the peak amplitude of the common mode current measurements. The incident E-field is shown in Fig. 5.

B. Differential mode voltage results

DM voltage tests were performed in each of the 9 cables while the raceway was either in the vertical or horizontal position. Three DM voltages were measured for each of the three LVP lines, namely, the Phase-Neutral voltage (PN), the Phase-Ground voltage (PG), and the Neutral-Ground voltage (NG). In the case of the TEL and LAN cables, the DM voltage was measured between the pins indicated in Fig. 2.

1) Typical result

The DM voltages obtained in the AC3 cable while the raceway was in the vertical position are presented in Fig. 12. The peak amplitudes of the PN (in red), PG (in green), and NG (in blue), were 160 V, 460 V and 470 V, respectively. Similar curves exhibiting an oscillatory behavior with several resonant frequencies were obtained for the other cables.

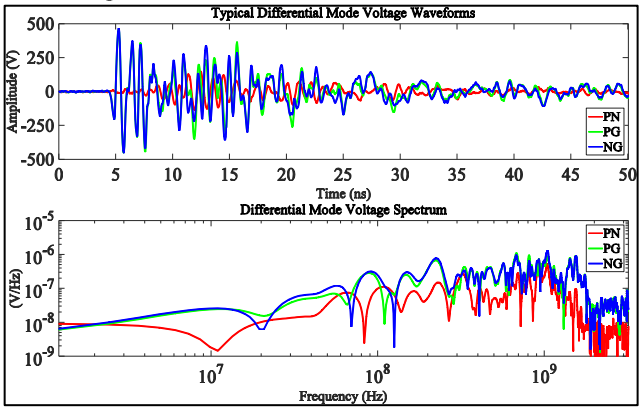

Fig. 12 Example of a differential mode voltage measurement of the AC3 cable with the raceway in a vertical position. The incident E-field is shown in Fig. 5.

2) Peak amplitudes

A bar plot summarizing the peak amplitudes of the DM voltage measurements of all the cables is presented in Fig. 13. The PN, PG, and NG voltage amplitudes of the LVP cables are plotted with a continuous, dashed, and dotted line, respectively.

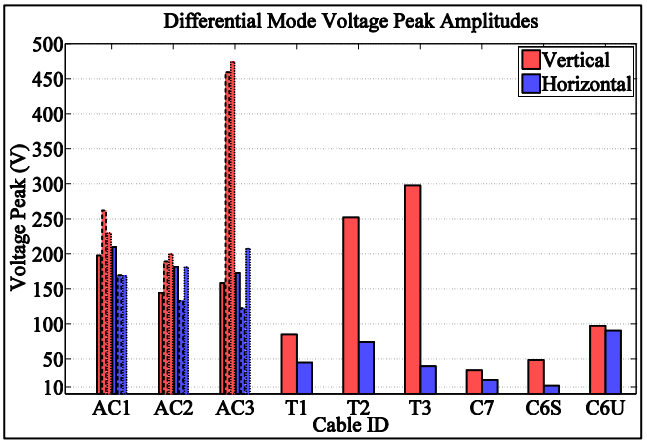

Fig. 13 Bar plot of the peak amplitude of the DM voltage measurements. The incident E-field is shown in Fig. 5.

It was found that almost all the induced voltages in the LVP cables remained in the range of 120-250V. Notice that there are two cases in AC3 with induced voltages of more than 450V that significantly differ from the others. Peak voltages between 40-300V were obtained for the TEL cables and between 10-100 V for the LAN cables. Similar levels were obtained for hyperband testing (at 44kV/m) of an unshielded CAT5 cable in [1].

The highest amplitudes were obtained with the raceway in the vertical position. The influence of the shielding scheme of the LAN cables can be also observed: reduced peak voltages are obtained for the shielded cables (C6S and C7).

VI. Differential Mode Voltage Transfer Functions

In order to address the overall shielding effectiveness of the assembly of cables, patch cords and measurement cards, the electric field to DM voltage transfer functions were calculated. Unless specified, all the transfer functions contain the overall coupling contribution from the raceway, the patch cords, and the measurement cards. The measurement cards play the role of typically found connector terminals through which EM energy can be also coupled. The obtained transfer functions give an idea of the required protection for limiting the induced voltage at the equipment terminals.

A. Transfer function definitions

1) Low frequency band (40MHz -200MHz)

The transfer functions between 40MHz and 200MHz were calculated by using the Fourier decomposition of the DM voltage and the illuminating field measured during the HPEM tests. The magnitude of the DM transfer functions $|H_{V_d}|$ were obtained from:

$$|H_{V_d}| = \left|\frac{V_{DM}}{E^{inc}}\right|, \qquad (3)$$

in which V_{DM} is the Fourier spectrum of the measured DM voltage between two wires of the tested cables (see Fig. 2) while the raceway was in the vertical position, and E^{inc} is the Fourier spectrum of the generated field inside the GTEM cell working volume. The reason for not using the horizontal measurements for the transfer function calculation is that the incident field along the raceway cannot be described with a single reference measurement (as done for the vertical case), due to the 1/r dependence of the amplitude in the longitudinal dimension of the GTEM cell. Notice that for the LVP cables, the DM voltage was measured between the phase and neutral wires. The lower frequency limit of the measurement was given by the number of samples in the time window and the sampling rate of the oscilloscope used.

2) High frequency band (200 MHz-6GHz)

The transfer functions between 200 MHz and 6 GHz were calculated by using the results obtained in the RC. The following definition of the transfer function was used:

$$|H_{V_d}| = \sqrt{\frac{\langle |V_{DM}|^2 \rangle}{\langle |E^{inc}|^2 \rangle}}, \qquad (4)$$

where $\langle |V_{DM}|^2 \rangle$ and $\langle |E^{inc}|^2 \rangle$ have been already defined in (1) and (2).

B. Transfer function results

Given that the nature of the transfer functions definitions is different, a priori, a consistent average transfer function value among both methods is not expected. However, according to the results of [16] the average transfer function of a plane wave illumination test should be, within a few decibels, equal to the transfer function in a reverberation chamber. As it is shown later, there is a broad consistency in the average coupling level between the low and high frequency band transfer functions. However, regarding the transition at 200 MHz, differences between 6 to 20dBs have been found.

The obtained transfer functions feature a strong variation as a function of frequency and they do not follow a common pattern. However, depending on the cable nature (untwisted, twisted, or shielded), it has been found that the transfer functions have similar behaviors as will be presented in what follows.

The magnitudes of the transfer functions of two LVP cables (AC1 and AC3), two TEL cables (T1 and T3), and two LAN cables (C7 and C6U), are plotted in Fig. 14, Fig. 15, and Fig. 16, respectively.

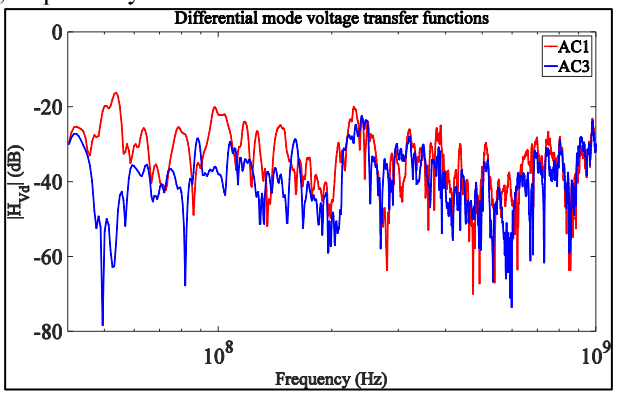

Fig. 14 Magnitude of the DM voltage transfer function of the AC1 and AC3 LVP cables.

The LVP cables exhibit the strongest response with the magnitude of the transfer functions reaching about -20 dB at the resonant frequencies (Fig. 14). Twisted cables with no

overshield, like the TEL cables or the C6U cable, have an improved behavior with respect to the untwisted, with a magnitude of about -30 dB at the resonant frequencies (Fig. 15 and Fig. 16). The lowest response is obtained with the C7 cable (twisted and shielded) with nearly -40 dB at the resonant frequencies.

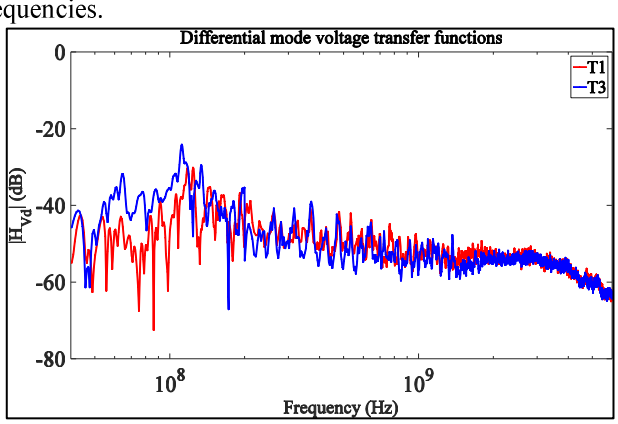

Fig. 15 Magnitude of the DM voltage transfer function of the T1 and T3 TEL cables.

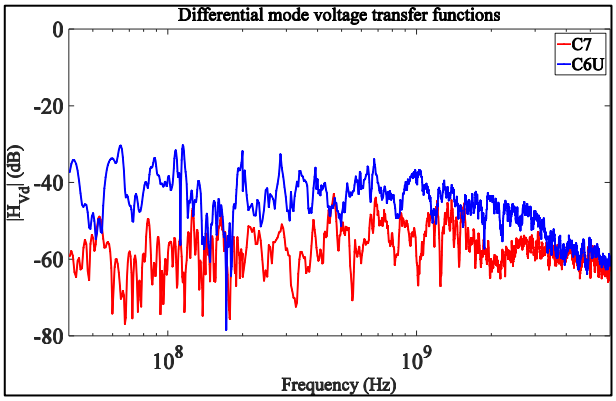

Fig. 16 Magnitude of the DM voltage transfer function of the C7 and C6U LAN cables.

A summary of the maximum, minimum and mean transfer functions for all the tested cables considering the whole frequency range is presented in Fig. 17. In this plot, the improved response of the twisted and shielded cables can be easily appreciated.

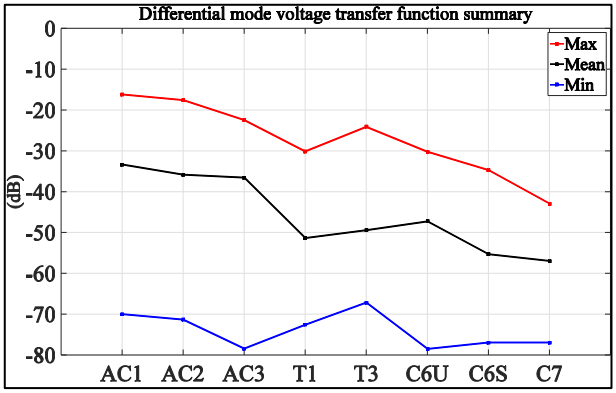

Fig. 17 Maximum, minimum, and mean amplitudes of the DM voltage transfer functions measured in all the cable types of the raceway

Theoretical models leading to the correct prediction of the DM mode coupling require very detailed information about the geometry and imperfections in the line terminations (see e.g. [19, 22]). Given the many uncontrolled parameters of our assembly, we have chosen to compare our results with comparable experiments reported in the literature.

Similar measurements were performed with home-made unshielded TWP of arbitrary wire separation distance by using a CW illumination in an AC in [17, 18, 22] and a RC in [21]. Contrary to our case, in these experiments a very careful termination of the wires has been made; e.g. the experiments in [21] and [22] used baluns for terminating the wires, thus reducing the CM to DM conversion.

We have tried to obtain the equivalent DM voltage transfer functions from the information provided in the cited papers. The AC results in [17, 18] and [22] exhibit levels of about -90 to -50 dB, and -80 to -40 dB, respectively. In these two examples, the TWP separation distances were around 1-2 mm and they were illuminated from particular angles of incidence. Therefore, the statistical significance of the measurements was low.

On the other hand, the RC results in [21] show transfer functions between -60 and -20 dB. In this case, the TWP separation distances were 16mm and 33.7mm, and this explains the higher coupling levels with respect to the AC examples. Also, the multiple angles of incidence imply an increased probability of exciting the TWP with illumination conditions that will be difficult to obtain with an AC test.

C. Discussion

In this section we present some additional measurement results that are useful for explaining the governing factors in the transfer functions. The results presented in Fig. 17 show that the type of cable has, in general, an appreciable effect on the obtained transfer functions; the unshielded-untwisted cables being the most susceptible, and the shielded-twisted cables the least susceptible wires (as expected). However, the difference between the transfer functions of the TEL and LAN cables becomes less significant at higher frequencies. Given that the observed transfer functions contain the joint effect of the measurement cards, the patch cords used to access the raceway, and the raceway cables, it is expected that at higher frequencies the majority of the energy penetrates through imperfections in the cable terminations or couples directly to the measurement cards. Thus, similar responses are obtained at higher frequencies.

We have performed further measurements in the RC in order to identify the governing effects in the total system response. We measured the transfer functions of the measurement cards by themselves, and with just patch cords between them (without the raceway). An example of the obtained results is presented in Fig. 18 which compares the magnitude of the transfer function of one measurement card alone (MC), two measurement cards with just a C7 shielded patch cord in between them (C7-PC), and the full measurement system connected to the C7 cable of the raceway (C7).

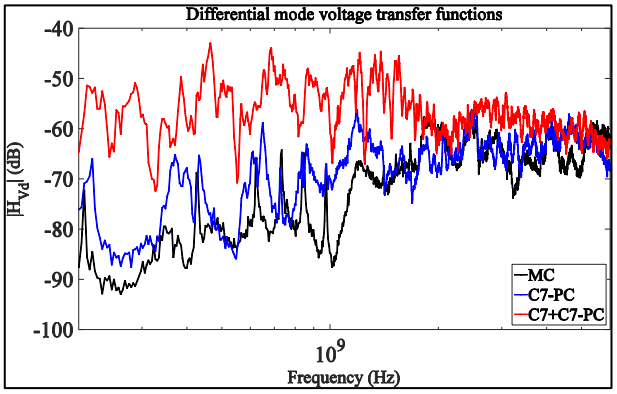

Fig. 18 Magnitude of the DM voltage transfer function measured in the C7 cable, the C7 patch cord, and the measurement card alone.

According to Fig. 18, below a frequency of about 1 GHz, the cable coupling is dominant. Beyond a frequency of about 2 GHz, direct coupling to the measurement cards become predominant. A similar behavior was observed for the other cables.

In order to separate the effect of the measurement cards and that of the connected cables, the maximum, minimum, and mean transfer functions were calculated in two separate frequency bands; namely, 0.2 to 2 GHz, and 2-6 GHz. A summary of the results is presented in Fig. 19, in which the transfer functions of a measurement card alone (MC) and, two measurement cards connected through patch cords (CX-PC) have been added. Notice that the statistical moments of the second band feature less variation as a function of the considered configuration compared to the first band, meaning that the coupling is independent of the cable type and is essentially governed by the measurement cards (± 5 dBs).

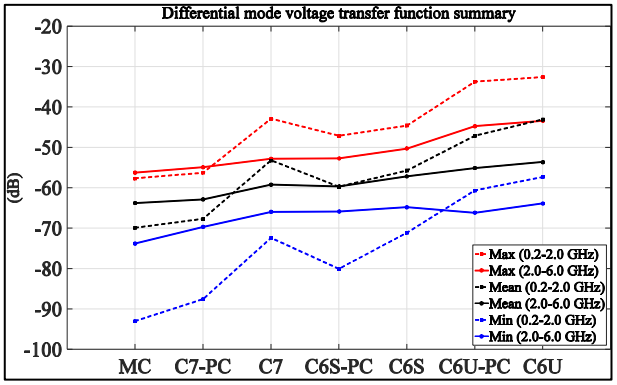

Fig. 19 Maximum, minimum, and mean amplitudes of the DM voltage transfer functions according to the analyzed frequency band

D. Effect of shield discontinuities

In order to assess the effect of inserting discontinuities in the shields, two tests were performed. In the first test, the transfer function of the measurement card alone without the copper seal in the RJ-45 jack was determined. A plot comparing the obtained results with the results of the former card with a continuous shield is presented in Fig. 20. The results with the unshielded connector card are plotted in red (MC-NS), and those with the shielded connector card are shown in black (MC). The transfer functions feature resonances which are presumably related to the PCB size and trace lengths. The observed resonance frequencies are specific to the particular MCs but it is expected that similar effects would occur in real equipment. A difference of about 15 dB is observed between the two curves.

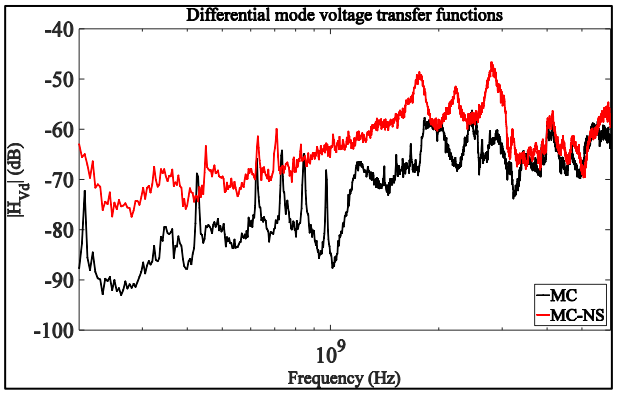

Fig. 20 Magnitude of the DM voltage transfer function measured in the measurement card alone with and without over shielding of the RJ-45 jack.

The second test consisted of testing the shielded cables of the raceway while connecting the measurement cards with and without shielded patch cords. The insertion of an unshielded patch cord introduced a discontinuity that degraded the performance of the entire system.

A plot comparing the response of the C7 cable of the raceway connected through shielded patch cords (C7+C7-PC), through unshielded patch cords (C7+C6U-PC), and the response of the C6U cable of the raceway connected through C6 unshielded patch cords (C6U+C6U-PC) is presented in Fig. 21. Notice that the presence of an unshielded patch cord degrades the response of the C7 cable so that it becomes similar to the response of an unshielded cable.

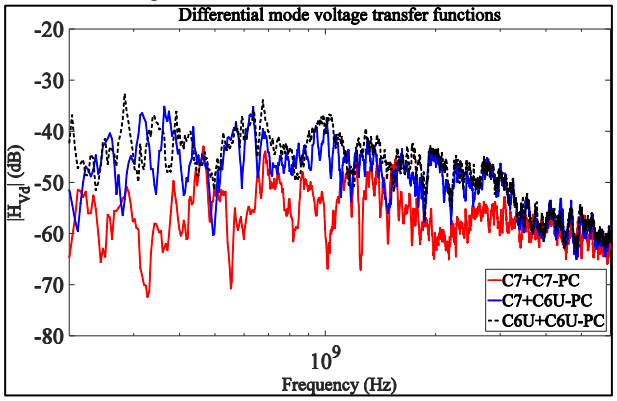

Fig. 21 Magnitude of the DM voltage transfer function measured in the C7 cable, the C7 cable with an unshielded patch cord, and the C6U cable.

VII. Conclusion

A typical electrical and communications raceway including several types of cables found in commercial buildings was built and tested against HPEM transients inside a GTEM cell and low power fields inside a RC. In the first test, the raceway was illuminated with a fast transient bipolar E-field pulse of ± 20kV/m and 100 ps rise-time, and the amplitude and frequency characteristics of the induced CM currents and DM voltages between the cable terminations were assessed.

The HPEM tests revealed that the low voltage power cables are the most susceptible under a hyperband illumination, compared to telephone and Ethernet cables.

Table V shows the range of the measured peak values in both tests (raceway in vertical and horizontal positions) and for each type of cabling.

TABLE V
MEASURED RANGE FOR THE INDUCED CM CURRENT AND DM VOLTAGE PEAKS. THE INCIDENT E-FIELD IS A HYPERBAND SOURCE WITH A PEAK-TO-PEAK VALUE OF 20 KV/M AND A RISETIME OF 100 PS.

Cable	Current range (A)	Voltage range (V)
LVP	2.1-8.5	122-474
TEL	1.7-9.8	40-298
LAN C6U (no shield)	2.2-5.6	91-107
LAN C6S (shielded)	4.4-6.8	10-49
LAN C7 (shielded)	4-6.8	13-34

In general, the amplitude of the induced CM current signals is related to the illuminated portion of the cables. On the other hand, the DM voltages are related to the illuminated portion, the presence or not of a shield, the load balance, and proper terminations of the cables. As expected, the best performance was obtained with the use of shielded twisted pairs.

In the second test, the response of the raceway to low power swept CW stimulation was measured in a RC to determine statistical transfer functions from random incident field configurations into DM voltage in cable loads. The obtained electric field to DM voltage transfer functions were summarized in Fig. 19. The responses were found to be governed by the raceway under test in the lower frequencies (below 1 GHz). Between 0.2-1 GHz, the raceway gives about 10 dB higher coupling than a short patch cable. The difference is even greater at lower frequencies and for shielded cables. In the frequency band 1-3 GHz, little differences were observed between a short patch cable and full raceway, but both are still significantly higher than direct coupling to the measurement card. Beyond 3 GHz, the coupling is clearly dominated by the measurement cards.

The experiments performed in this work provide a better understanding of the expected induced voltages and currents in commercial cable systems when exposed to IEMI-like signals. For the first time in the literature, three types of cabling (plus 3 subtypes of Ethernet) were investigated using an identical experimental technique in a very broad frequency range, namely from 40 MHz to 6 GHz. The considered cabling configuration was in a representative installed environment (raceway) rather than just individual cables. The GTEM and RC test results in the cross-over region were found to be broadly consistent. The transfer functions derived in this work are therefore directly useful in IEMI risk analyses for many types of critical infrastructures, bearing in mind, of course, that they are derived from particular experiments.

ACKNOWLEDGMENT

The authors are grateful to Dr. Carlos Romero (EPFL) for the support in the design and construction of the measurement cards.

REFERENCES

[1] F. Brauer, F. Sabath, and J. L. ter Haseborg, "Susceptibility of IT network systems to interferences by HPEM," in *Electromagnetic Compatibility, 2009. EMC 2009. IEEE International Symposium on*, 2009, pp. 237-242.

[2] F. Brauer, S. Fahlbusch, J. L. ter Haseborg, and S. Potthast, "Investigation of Hardening Measures for IT Equipment against Radiated and Conducted IEMI," *Electromagnetic Compatibility, IEEE Transactions on,* vol. 54, pp. 1055-1065, 2012.

[3] M. Kreitlow, H. Garbe, and F. Sabath, "Influence of software effects on the susceptibility of Ethernet connections," in *Electromagnetic Compatibility (EMC), 2014 IEEE International Symposium on*, 2014, pp. 544-548.

[4] D. V. Giri and F. M. Tesche, "Classification of intentional electromagnetic environments (IEME)," *Electromagnetic Compatibility, IEEE Transactions on,* vol. 46, pp. 322-328, 2004.

[5] C. R. Paul, *Analysis of multiconductor transmission lines.* Hoboken, N.J.: Wiley-Interscience : IEEE Press, 2008.

[6] F. M. Tesche, M. V. Ianoz, and T. Karlsson, *EMC analysis methods and computational models.* New York: Wiley, 1997.

[7] S. A. Pignari and G. Spadacini, "Plane-Wave Coupling to a Twisted-Wire Pair Above Ground," *Electromagnetic Compatibility, IEEE Transactions on,* vol. 53, pp. 508-523, 2011.

[8] F. Rachidi, "A Review of Field-to-Transmission Line Coupling Models With Special Emphasis to Lightning-Induced Voltages on Overhead Lines," *Electromagnetic Compatibility, IEEE Transactions on,* vol. 54, pp. 898-911, 2012.

[9] N. Mora, C. Kasmi, F. Rachidi, M. Darces, and M. Helier, "Modeling of the propagation along low voltage power networks for IEMI studies," in *Electromagnetics in Advanced Applications (ICEAA), 2013 International Conference on*, 2013, pp. 436-439.

[10] N. Mora, C. Kasmi, F. Rachidi, M. Darces, M. Hélier, and M. Rubinstein, "Analysis of the Propagation of High Frequency Disturbances along Low-Voltage Test Raceway," presented at the American Electromagnetics International Symposium (AMEREM), Albuquerque, New Mexico, USA, 2014.

[11] I. Junqua, J. P. Parmantier, and P. Degauque, "Field-to-Wire Coupling in an Electrically Large Cavity: A Semianalytic Solution," *Electromagnetic Compatibility, IEEE Transactions on,* vol. 52, pp. 1034-1040, 2010.

[12] M. Magdowski, S. V. Tkachenko, and R. Vick, "Coupling of Stochastic Electromagnetic Fields to a Transmission Line in a Reverberation Chamber," *Electromagnetic Compatibility, IEEE Transactions on,* vol. 53, pp. 308-317, 2011.

[13] G. Spadacini, F. Grassi, and S. A. Pignari, "Field-to-Wire Coupling Model for the Common Mode in Random Bundles of Twisted-Wire Pairs," *Electromagnetic Compatibility, IEEE Transactions on,* vol. 57, pp. 1246-1254, 2015.

[14] E. Genender, A. Kreth, D. Zamow, H. Garbe, and S. Potthast, "Combination of the failure probability with a random angle of incidence of the radiated interference," in *General Assembly and Scientific Symposium, 2011 XXXth URSI*, 2011, pp. 1-4.

[15] C. E. Baum, "Aspects of Random-Lay Multiconductor Cable Propagation Which Are Not Statistical," *Interaction Notes,* vol. 595, 2004.

[16] S. Silfverskiold, M. Backstrom, and J. Loren, "Microwave field-to-wire coupling measurements in anechoic and reverberation chambers," *Electromagnetic Compatibility, IEEE Transactions on,* vol. 44, pp. 222-232, 2002.

[17] R. B. Armenta and C. D. Sarris, "Efficient Evaluation of the Terminal Response of a Twisted-Wire Pair Excited by a Plane-Wave Electromagnetic Field," *Electromagnetic Compatibility, IEEE Transactions on,* vol. 49, pp. 698-707, 2007.

[18] R. B. Armenta and C. D. Sarris, "Modeling the Terminal Response of a Bundle of Twisted-Wire Pairs Excited by a Plane Wave," *Electromagnetic Compatibility, IEEE Transactions on,* vol. 49, pp. 901-913, 2007.

[19] G. Spadacini and S. A. Pignari, "Numerical Assessment of Radiated Susceptibility of Twisted-Wire Pairs With Random Nonuniform Twisting," *Electromagnetic Compatibility, IEEE Transactions on,* vol. 55, pp. 956-964, 2013.

[20] M. Magdowski and R. Vick, "Simulation of the stochastic electromagnetic field coupling to an unshielded twisted pair of wires," in *Electromagnetic Compatibility (EMC), 2013 IEEE International Symposium on*, 2013, pp. 33-37.

[21] M. Magdowski, J. Ladbury, C. Holloway, and R. Vick, "Measurement of the stochastic electromagnetic field coupling to an unshielded twisted pair cable," in *Electromagnetic Compatibility (EMC Europe), 2014 International Symposium on*, 2014, pp. 659-664.

[22] G. Spadacini, S. A. Pignari, and F. Marliani, "Experimental measurement of the response of a twisted-wire pair exposed to a plane-wave field," in *Electromagnetic Compatibility (EMC), 2011 IEEE International Symposium on*, 2011, pp. 828-833.

[23] F. Grassi, G. Spadacini, and S. A. Pignari, "The Concept of Weak Imbalance and Its Role in the Emissions and Immunity of Differential Lines," *Electromagnetic Compatibility, IEEE Transactions on,* vol. 55, pp. 1346-1349, 2013.

[24] G. Spadacini, F. Grassi, and S. A. Pignari, "On the combined effect of random nonuniformity and deformation of twisting on the radiated immunity of twisted-wire pairs," in *Electromagnetic Compatibility (EMC), 2013 IEEE International Symposium on*, 2013, pp. 489-493.

[25] C. Jullien, P. Besnier, M. Dunand, and I. Junqua, "Advanced Modeling of Crosstalk Between an Unshielded Twisted Pair Cable and an Unshielded Wire Above a Ground Plane," *Electromagnetic Compatibility, IEEE Transactions on,* vol. 55, pp. 183-194, 2013.

[26] C. Jullien, "Contribution à l'analyse et à la modélisation des couplages électromagnétiques au sein de torons de câbles à grand nombre de liaisons – Application aux câblages aéronautiques," Docteur de l'INSA de Rennes, Electronique et Télécommunications, Institut National des Sciences Appliquées de Rennes, Rennes, 2013.

[27] N. Mora, F. Rachidi, P. Pelissou, and A. Junge, "Numerical Simulation of the Overall Transfer Impedance of Shielded Spacecraft Harness Cable Assemblies," *Electromagnetic Compatibility, IEEE Transactions on,* vol. 57, pp. 894-902, 2015.

[28] M. Backstrom, T. Nilsson, and B. Vallhagen, "Guideline for HPM protection and verification based on the method of power balance," in *Electromagnetic Compatibility (EMC Europe), 2014 International Symposium on*, 2014, pp. 128-133.

[29] P. Delmote, J. P. Duperoux, F. Bieth, and S. Pinguet, "UWB HPM at ISL: The GIMLI project and other applications," in *High Power Microwave Defense & Security Workshop*, Saint-Louis, France, 2011.

[30] D. V. Giri and M. Nyffeler, "Pulse Adaptor for GTEM-3750 " presented at the 2011 Armasuisse HPE Workshop, Thun, Switzerland, 2011.

[31] A. C. Marvin, G. Esposito, J. F. Dawson, I. D. Flintoft, L. Dawson, J. A. K. Everard, and G. C. R. Melia, "A wide-band hybrid antenna for use in reverberation chambers," in *Electromagnetic Compatibility (EMC), 2013 IEEE International Symposium on*, 2013, pp. 222-226.

[32] IEC, "61000-4-21: Electromagnetic compatibility (EMC) - Part 4-21: Testing and measurement techniques - Reverberation chamber test methods," ed: IEC, 2011.

[33] J. G. Kostas and B. Boverie, "Statistical model for a mode-stirred chamber," *Electromagnetic Compatibility, IEEE Transactions on,* vol. 33, pp. 366-370, 1991.

[34] L. Musso, V. Berat, F. Canavero, and B. Démoulin, "A plane wave monte carlo simulation method for reverberation chambers," in *Int. Symp. Electromagn. Compat. EMC Europe 2002*, Sorrento, Italy, 2002, pp. 45-50.

[35] R. Rambousky, A. Bausen, L. O. Fichte, and F. Sabath, "HPEM susceptibility testing using a special infrastructure facility," in *Future Security 2013*, Berlin, 2013.